Exploration of Configuration Options for a Large Civil Compound Helicopter

Carl Russell and Wayne Johnson
Aeromechanics Branch
National Aeronautics and Space Administration
Ames Research Center, Moffett Field, California
carl.russell@nasa.gov, wayne.johnson@nasa.gov

ABSTRACT

Four 90-passenger compound helicopter configurations designed for a 500 nm transport mission are presented. The designs include a tandem configuration and three single-main-rotor configurations, which use either propellers or a swiveling tail rotor for supplemental forward thrust in cruise. For this study, the sizing code NDARC and the comprehensive analysis code CAMRAD II were used for rotorcraft design tasks and detailed rotor analysis, respectively. The comprehensive analysis was used to calibrate rotor performance models for the sizing software, as well as determine the optimal distribution of lift between the wing and rotor. Results from both the conceptual design phase and the rotor analysis are presented. Parametric sweeps were performed to determine the optimum rotor and wing dimensions for the different compound helicopter configurations. Multiple metrics were used to determine the best configuration, with heavy emphasis on minimizing fuel burn. The results suggest that a compound helicopter using two lifting rotors in a tandem configuration provides the best performance in terms of empty weight, engine power, and fuel burn.

NOMENCLATURE

Acronyms

CH90	Baseline compound helicopter
ISA	International Standard Atmosphere
OGE	Out of ground effect
OEI	One engine inoperative
SC90	Swiveling tail rotor compound helicopter
SW90	Small-wing compound helicopter
TC90	Tandem compound helicopter

Symbols

A_{wing}	Wing aspect ratio
C_T	Rotor thrust coefficient
C_W	Weight coefficient
$c_{d\,mean}$	Rotor mean blade drag coefficient
D	Drag
e	Oswald efficiency
L	Lift
L/D_e	Effective lift-to-drag ratio, WV/P
P	Power
q	Dynamic pressure
S	Wing planform area
V	Forward speed
V_{br}	Speed for best range
W	Rotorcraft weight
η_{prop}	Propulsive efficiency
κ	Induced power factor
μ	Edgewise advance ratio
σ	Rotor solidity (thrust weighted)

Presented at the American Helicopter Society 69th Annual Forum, May 21-23, 2013.

INTRODUCTION

Vertical and short takeoff and landing (V/STOL) aircraft are one possible solution for increasing airport throughput without causing increased flight delays or requiring significant improvements at airports (Refs. 1-2). Short-haul regional flights represent the likely target market for large V/STOL passenger aircraft. For design missions with a range on the order of 1,000 nm, the NASA Heavy Lift Rotorcraft Systems Investigation (Ref. 3) showed that while a tiltrotor configuration provides the best vertical takeoff solution, a compound helicopter is a promising alternative meriting further investigation.

A more recent study examined whether a compound helicopter would perform better than either a conventional helicopter or a tiltrotor for a 500 nm design mission and found that the tiltrotor still retained a lower empty weight, engine power, and fuel burn than the compound (Ref. 4). One limitation of that study was that while there are many configuration options for a compound helicopter, the analysis focused on a single concept. The study presented here more fully explored the compound helicopter design space. Using a consistent set of assumptions and design methodology, multiple configurations were examined in an effort to determine the advantages and disadvantages of different compounding methods.

To evaluate the different configurations, four compound helicopter designs were created using NASA's rotorcraft design code NDARC. Detailed rotor performance analysis was carried out with the CAMRAD II comprehensive rotorcraft analysis code. Each aircraft design is capable of carrying a payload of 90 passengers, or 19,800 lb, over a range of 500 nm. The designs use the same fuselage geometry so that passenger accommodation is consistent. They also use the same scalable engine performance model. Aside from the fuselage, payload, and engine specifications, the four aircraft designs are independent.

BACKGROUND: COMPOUND HELICOPTERS

Conventional helicopters are limited to cruise flight speeds of approximately 170 kt because retreating blade stall severely limits lift and propulsive thrust at higher speeds. There are multiple methods of compounding a helicopter to achieve flight speeds well above this limit. With lift compounding, a wing is added to the aircraft to unload the main rotor. Thrust compounding adds a propulsor, such as a propeller or jet engine, to provide the necessary thrust for high speeds. Compressibility drag on the advancing side of the main rotor limits forward speed as the advancing tip Mach number approaches sonic conditions. Therefore, the rotational speed of the rotor must be reduced in high-speed flight to mitigate this effect.

Various compound helicopter configurations have been built and experimented with over the years, but none have been mass-produced; the AH-56 Cheyenne (Ref. 5), the Sikorsky X2 (Ref. 6), and the Eurocopter X3 (Ref. 7) are three prominent examples. Recently, design studies have focused on compound helicopters for military applications, including heavy-lift and joint-services missions (Refs. 8-11). All of these designs incorporate different compounding methods to achieve higher speeds than conventional helicopters are capable of.

The multitude of available compounding methods can make for a very large design space. It would be infeasible to investigate all of the possibilities. The current study focused on four possible configurations by incorporating a subset of compounding technologies to enable efficient high-speed passenger transport.

APPROACH

Configurations

The compound helicopter studied in Ref. 4 provided the baseline for comparisons and is referred to as CH90 in this paper. Including the baseline, the following compound helicopter configurations were studied:

1. **Baseline (CH90):** Fully compounded, with a slowed single main rotor and tail rotor, and auxiliary propulsion provided by two propellers mounted on a large high-aspect ratio wing.
2. **Swiveling Tail Rotor Compound (SC90):** Similar to the baseline CH90 configuration, but instead of wing-mounted propellers for auxiliary propulsion, the tail rotor swivels to become a propeller in cruise.
3. **Small-Wing Compound (SW90):** Similar to the SC90, but with a much smaller wing and a larger share of the lift carried by the main rotor.
4. **Tandem Compound (TC90):** Two counter-rotating lifting rotors in a tandem configuration with auxiliary propulsion provided by two wing-mounted propellers. A large high-aspect ratio wing provides supplemental lift in cruise.

Other configurations were also considered. Aircraft using lift-offset rotors, such as the Sikorsky X2, are a promising alternative for smaller designs; however, the results of Ref. 3 suggested that a lift-offset rotor would not be a good candidate for the size of aircraft studied here. Another possible configuration would eliminate the tail rotor on the CH90 and use the propellers for anti-torque in hover, similar to the Eurocopter X3. This would require moving the propellers outboard on the wing, which would increase the wing weight. Also the propellers cannot be as large as a tail rotor, due to interference with the ground and the main rotor, so a higher hover efficiency was expected with an anti-torque tail rotor.

All of the designs use a slowed main rotor in cruise to avoid excessive compressibility drag on the advancing side. The single-main-rotor designs use a seven-bladed rotor similar to the rotors of existing large helicopters, such as the Sikorsky CH-53E. The tandem design uses two four-bladed rotors, similar to the tandem compound described in Ref. 3. The rotor optimization is discussed in the Results section.

The propellers use a performance model that gives a propulsive efficiency of approximately 0.88. Similar to the CH90 and TC90 propellers, the SC90 and SW90 tail rotors use an 8-bladed design, while the CH90 tail rotor has 5 blades. Detailed propeller design was outside the scope of this study, but would certainly be needed for further refinements of any of these configurations.

All of the designs use a wing that has a fixed incidence relative to the fuselage, but has hover flaps over almost the entire span. For the three large-wing designs, the wing dimensions were optimized by varying the wing loading at fixed aspect ratio. For the SW90, the wing dimensions were fixed, with a span of 50 ft. This makes the wingspan approximately half the main rotor diameter. Due to radial variation in downwash intensity, this reduction in wing size reduces the hover download on the wing by approximately 60% compared with the large-wing designs.

The levels of weight-saving technology assumed for all of the designs are consistent with those used in Ref. 3. The fuselage dimensions for the four configurations are identical

to those of NASA's 2nd generation Large Civil Tiltrotor (LCTR2), which is designed to carry 90 passengers (Ref. 12). The scalable engine model used for all four designs is the same as the LCTR2 engine model.

For all of the configurations, the propulsion group consists of four engines, and the total engine power can be delivered to the lifting rotors via a central gearbox in hover. In cruise, power is split between the main rotor(s) and the propeller(s). For the configurations with propellers on the wings (CH90 and TC90), the engines are located in nacelles behind the propellers. A cross shaft in the wing carries power from the engines to the central gearbox. For the SC90 and SW90, the engines are located on either side of the main gearbox.

Drawings showing the layouts of the four designs are given in Figs. 1-4.

Design Requirements

A single design mission was used to size the four configurations. The primary requirement of the design mission is transport of 90 passengers (19,800 lb) over a distance of 500 nm. The full mission description is given in Table. 1. In addition to the design mission, the aircraft were sized to two performance conditions: an OEI hover out of ground effect at design gross weight at 5,000 ft ISA+20°C and sea-level hover at maximum power. The first performance condition sized the engines, and the second sized the transmission.

There was no minimum speed requirement imposed on the designs, so the cruise speed was set at V_{br}, the speed for maximum range. There was also no required cruise altitude, and this parameter was varied during the design process.

Table 1. Design mission for all four designs

Design Mission
3 min taxi, 5k ISA +20˚C
2 min hover OGE 5k ISA +20˚C
Climb at maximum climb rate (credit distance to cruise segment)
Cruise at V_{br} for 500 nm range at best altitude
Descend at V_{br} (no range credit)
1 min hover OGE, 5k ISA +20˚C
Reserve (alternate airport): 100 nm V_{br} at cruise altitude
Reserve (emergency): 30 min V_{br} 5k ISA
Performance Requirements
One engine inoperative hover OGE at 5k ISA +20˚C
Max gross weight hover OGE at 0k ISA

Hover tip speed was limited for all the designs to 650 ft/s to minimize takeoff noise. The design C_w/σ was set by maneuver requirements for a tiltrotor, determined by Ref. 13. The assumption here is that, like a tiltrotor, a compound helicopter will be flying on both the main rotor and the wing during its most demanding maneuvers, so the rotor solidity requirements will be similar.

Design Process

The iterative design process used for this study is illustrated in Fig. 5. Tasks of the design process utilizing NDARC are contained in the heavier square boxes, while tasks using CAMRAD II are contained in the lighter rounded boxes. The rounded boxes with dashed lines indicate tasks that used a combination of CAMRAD II and spreadsheet analysis. Data passed between steps is identified next to the flowchart arrows. The process for each of the different configurations was the same, and the steps are outlined below.

1. Sweep aircraft parameters
   Aircraft characteristics such as wing loading, disk loading, and cruise altitude were varied in NDARC using a baseline rotor model, resulting in an initial configuration.

2. Analyze rotors with varied twist distributions
   Using the rotor diameter and solidity determined in Step 1, rotors with varying blade twists were simulated in CAMRAD II at the design mission cruise and hover conditions to develop a set of candidate rotors.

3. Re-size aircraft for different twist distributions
   The κ and $c_{d\,mean}$ determined in Step 2 for each of the candidate rotors were used in NDARC to re-size the aircraft. The rotor blade twist was chosen based on the candidate rotor that minimized fuel burn, empty weight, and engine power.

4. Determine optimal lift share in cruise
   The main rotor shaft angle was varied at fixed collective, and spreadsheet calculations were used to determine the optimal lift share for maximum lift-to-drag ratio in cruise.

5. Generate updated rotor performance model
   Using the rotor twist distribution determined in Step 3, various flight conditions were simulated in CAMRAD II to generate a math model of the rotor power consumption. While the κ and $c_{d\,mean}$ determined in step 3 were for only two specific flight conditions, the performance model determined here spanned the expected range of operating conditions for the aircraft.

6. Sweep aircraft parameters 2
   Using the rotor performance model generated in Step 5, aircraft characteristics were swept again to arrive at a revised configuration. Steps 2-5 could be repeated multiple times if necessary. For this study, the loop was only completed once for each aircraft.

7. Off-design analysis
   Once the final aircraft design was determined, NDARC was used to analyze different operating conditions and missions.

Computational Methods – Sizing

All of the sizing and design tasks were carried out using NASA's rotorcraft design code NDARC. NDARC is a conceptual/preliminary design and analysis code for rapidly sizing and conducting performance analysis of new rotorcraft concepts (Refs. 14-16). NDARC has a modular code base, facilitating its extension to new concepts and the implementation of new computational procedures. NDARC Version 1.6 was used to generate the designs for this study.

A typical NDARC run consists of a sizing task, followed by off-design performance analysis. During the sizing process, point condition and mission performance are calculated and the aircraft is resized both geometrically and mechanically until the convergence criteria are met.

The software uses reduced-order performance models for various rotorcraft subsystems, such as rotors and engines, in order to facilitate short runtimes. These models require curve-fits to higher-fidelity models in order to accurately capture rotorcraft performance.

The NDARC rotor performance model represents the rotor power as the sum of induced, profile, and parasite terms: $P=P_i+P_o+P_p$. The parasite power (including climb/descent power for the aircraft) is obtained from the wind axis drag force and forward velocity: $P_p=-XV$. The induced power is calculated from the ideal power and the induced power factor κ: $P_i = \kappa P_{ideal}$. The profile power coefficient is calculated from a mean blade drag coefficient: $C_{Po} = (\sigma/8)c_{d\,mean}F_P$, where the function $F_P(\mu,\mu_z)$ (Ref. 17) accounts for the increase of the blade section velocity with rotor edgewise and axial speed.

There is a two-step process required to calculate induced and profile power in NDARC. First, use comprehensive analysis (CAMRAD II in this case) to calculate rotor performance for the full range of expected flight and operating conditions. Second, calibrate the parameters of the NDARC rotor performance model to match the calculated κ and $c_{d\,mean}$.

Computational Methods – Comprehensive Analysis

Performance analyses for rotor optimization were conducted with the comprehensive rotorcraft analysis CAMRAD II (Ref. 18). CAMRAD II is an aeromechanics analysis of rotorcraft that incorporates a combination of advanced technologies, including multibody dynamics, nonlinear finite elements, and rotorcraft aerodynamics. The trim task finds the equilibrium solution for a steady state operating condition, and produces the solution for performance and loads. The aerodynamic model includes a wake analysis to calculate the rotor non-uniform induced velocities. CAMRAD II has undergone extensive correlation of performance and loads measurements on helicopters, detailed in Refs. 19-26.

The CAMRAD II aerodynamic model for the rotor blade is based on lifting-line theory, using steady two-dimensional airfoil characteristics and a vortex wake model. The wake analysis calculates the rotor non-uniform induced velocity using either rigid or free wake geometry. The concentrated tip vortices are the key features of the rotor wake, important for calculating performance and airloads.

For this study, rotor performance optimization in CAMRAD II considered a single main rotor for each of the four designs, and the calculations for calibration of the NDARC rotor model assumed an isolated rotor. Interference effects of the wing on the rotor in cruise were assumed to be negligible, based on results from Ref. 9. For the TC90 design, interference between the two rotors was modeled when determining the optimum lift share between the wing and rotors in cruise. Those results will be discussed later. Rotor performance was calculated assuming elastic blades. Non-uniform inflow with rigid wake geometry was used for high-speed cruise and free wake geometry was used in hover. Airfoil characteristics were obtained from tables representing advanced technology airfoils.

For calibration of the NDARC performance model, various parameters were swept for cruise and hover conditions. In hover, C_T/σ was swept through the range of expected thrust values. In cruise, thrust and velocity were varied through the expected envelope of operations for each of the four compound helicopter designs.

Trim Schemes

Both NDARC and CAMRAD II contain trim tasks that find an equilibrium point for either the entire aircraft or a single rotor. In the case of a compound helicopter, the lift share between the rotor and wing must be trimmed in cruise. This results in seven trim targets, including the usual six forces and moments. For this study, the main rotor collective and aircraft pitch angle were used to trim total lift and wing lift share in NDARC.

The single-rotor cases in CAMRAD II had simple trim schemes, with cyclic pitch trimming the rotor to zero flapping and rotor shaft angle trimming thrust at fixed collective. For the tandem designs, the rotor simulations for determining lift share were executed with two rotors, and there was a small effect from interference. In order to achieve the same thrust on both rotors, a six-variable trim scheme was required. Flapping was trimmed by individual cyclic controls on the rotors. Thrust was trimmed on the front rotor by varying shaft angle at fixed collective. Collective pitch on the rear rotor was varied to match the same thrust as the front rotor. Downwash effects from the front rotor resulted in a higher collective on the rear rotor to trim thrust, so the shaft angle of the rear rotor was varied manually until the collective values were approximately equal. This resulted in the rear rotor incidence being one degree more than that of the front rotor.

Cruise Efficiency

To determine the cruise efficiency of the aircraft designs at different rotor conditions, the effective lift to drag ratio must be calculated:

$$\frac{L}{D_e} = \frac{WV}{P}$$

L/D_e was calculated using a combination of results from both comprehensive analysis and the sizing code with a spreadsheet analysis. The weight W and speed V were known from NDARC, but the total power had to be determined. The power from the main rotor was output directly from CAMRAD II, and then the power to the propellers was calculated in a spreadsheet. First, the wing lift was determined by subtracting the rotor lift from the gross aircraft weight. The induced drag of the wing was then calculated as:

$$D_{wing,i} = \frac{qS}{\pi A_{wing} e}\left(\frac{L_{wing}}{qS}\right)^2$$

Oswald efficiency was assumed to be 0.8. The total drag was summed, including contributions from the rotor, wing, airframe, and any momentum drag or jet thrust from the engines. The only calculated drag effects due to changes in angle of attack came from the induced drag on the wing. Profile drag rise on the airframe due to angle of attack and induced drag on the tails were not included in the spreadsheet analysis, so the drag was slightly underestimated. The total power required, assuming a propulsive efficiency of the propellers and including drivetrain power losses, is:

$$P = \frac{DV}{\eta_{prop}} + P_{rotor} + P_{loss}$$

RESULTS

Table 2 summarizes key parameters for the four compound helicopter designs. Note that wing loading is referenced to the entire aircraft design gross weight. The disk loading for the single main rotor designs is referenced to design gross weight, and for the tandem, disk loading is referenced to 0.5×DGW. The weight breakdown of the four configurations is given in Table 3.

Rotor Design

Based on preliminary sizing runs, an expected cruise speed was used to target an advancing tip Mach number of approximately 0.85. This resulted in tip speeds of 450 ft/s for the SC90 and CH90, 475 ft/s for the TC90, and 550 ft/s for the SW90. Any follow-on work to this study should include a more rigorous optimization of the cruise tip speed.

Rotor twist optimization was performed three separate times: once each for the TC90, SW90, and SC90. The initial parameter sweeps (step 1 in the design process) used the rotor performance model previously developed for the baseline CH90 configuration. For the final designs and parameter sweeps (step 6 in the design process), updated models were used. Since the SC90 and CH90 have very similar main rotors, and fly at nearly the same conditions, these two designs have the same blade twist and share a single rotor performance model.

The twist variation simulation runs were executed at the preliminary design conditions given in table 4. A bi-linear twist was assumed with the transition point at 50% radius.

Table 4. Twist optimization design conditions

	SC90,CH90	SW90	TC90
Hover C_T/σ	0.163	0.158	0.156
Hover altitude, ft	5,000	5,000	5,000
Cruise C_T/σ	0.088	0.120	0.0652
Cruise altitude, ft	25,000	15,000	25,000
Cruise speed, kt	240	220	234
Cruise μ	0.90	0.675	0.832

Results for the rotor twist optimization are shown in Figs. 6-8. Outboard twist was swept from -21 deg/R to -3 deg/R, and inboard twist was swept from -6 deg/R to 6 deg/R. The inboard twist is indicated on Figs. 6-8 by the numbers next to the data points. Varying the twist will generally result in opposing changes in hover and cruise efficiency. For choosing optimum blade twist, hover efficiency was measured by the main rotor figure of merit, and cruise efficiency was measured by the aircraft effective lift-to-drag ratio.

The twist variation results form a Pareto front of maximum combined cruise and hover efficiency. Points on the Pareto front were chosen as test cases for NDARC; these selected points are identified by the circles in Figs. 6-8. The κ and $c_{d\,mean}$ for cruise and hover obtained from the comprehensive analysis for these points were input to the sizing code, and the aircraft were resized to determine which twist provided the lowest fuel burn, weight, and power. The optimum twist is indicated on each of the figures, and the twist distribution for the three rotors is shown in Fig. 9. The three rotors have similar twist characteristics. The CH90/SC90 rotor has an inboard twist of -3 deg/R and outboard twist of -18 deg/R. The SW90 optimum is -3 deg/R inboard and -15 deg/R outboard, and the TC90 optimum is 3 deg/R inboard and -15 deg/R outboard.

For the small wing design, SW90, the generally poor L/D_e of the configuration favors the twist for the highest possible cruise efficiency for minimum fuel burn, empty weight, and installed power. For the other designs, the twist selection is a balance between high hover efficiency for low empty weight and installed power, and high cruise efficiency for maximum L/D_e.

Rotor and Wing Lift Share

The optimum wing lift share was determined with a combination of CAMRAD II results and spreadsheet analysis. With the rotor twist determined, rotor shaft angle was varied for multiple values of rotor collective. Speed was held constant at the V_{br} determined in the preliminary sizing stage, and altitude was the same as that given in Table 4.

For the TC90 design, it was desirable to ensure that any interference effects were accounted for in determining the optimum lift share, so both rotors were modeled in CAMRAD II. The interference effects proved to be small; the power due to interference on the rear rotor was only 21 HP. The power to the main rotors in cruise is approximately 1% of the total power required, so the interference effects were deemed inconsequential. The remaining rotor analysis tasks for the TC90 assumed an isolated rotor.

The results of the lift share optimization process are shown in Figs. 10-12. The large-wing designs all have maximum L/D_e with approximately 85% of the lift carried by the wing and zero degrees collective pitch (measured at 75% rotor radius). The curves are fairly flat near the optimum and a difference of a few percent lift share in either direction results in less than a 1% change in cruise efficiency. A wing lift share of 85% was selected for all of the large-wing designs.

For the SW90 design, a rotor collective of 8° and wing lift share of 50% provided the best L/D_e. Lower values of collective resulted in nearly the same or slightly better cruise efficiency at 50% lift share on the wing, but required that the rotor fly at a higher shaft angle. In order to fly in this manner, the rotor would need to either be mounted on the fuselage at a high incidence angle, which would cause a high nose-down pitch angle in hover, and possibly mechanical interference between the rotor and fuselage, or it would require a movable hub, which would carry a large weight penalty. Neither of these characteristics was desirable, so the results for a collective of 8° were chosen.

The optimum rotor lift share was then used as a trim target in the sizing code. The angle between the rotor shaft and the wing was determined through spreadsheet analysis and input into the sizing code as well. The resulting wing and rotor incidence angles are included in Table 2.

Rotor Performance Model

The final step that required the use of comprehensive analysis was the determination of the rotor performance model coefficients used by NDARC. For all three rotors, C_T/σ was varied from 0.04 to 0.2 in hover, trimming thrust with rotor collective. Speed was swept from 170 kt to 280 kt for different values of C_T/σ, trimming the rotor thrust with shaft angle. The collective was fixed at 0° for the large wing designs and 8° for the SW90. For the CH90/SC90 rotor, C_T/σ was varied from 0.07 to 0.10; for the SW90, from 0.08 to 0.14; and for the TC90, from 0.03 to 0.08. These values bracketed the expected operating conditions for the four designs.

Curve fits were generated for the NDARC induced and profile power models based on the comprehensive analysis results, with particular focus on the operating conditions observed in the preliminary sizing runs. This curve-fitting technique has been used by numerous studies in the past and was first demonstrated and validated in Ref. 16.

Parameter Sweeps

With the rotor geometry and wing lift share determined, the final step in the design process was to re-run parameter sweeps in the sizing code. Disk loading, wing loading, and cruise altitude were the primary variables investigated. Figure 13 shows how empty weight and fuel burn are affected by cruise altitude for the four different designs. Fuel burn is represented by the dashed lines, and empty weight is indicated by the solid lines. Installed engine power was also considered, and the trends are the same as those for empty weight and cruise altitude, so those results are not plotted here.

The three large-wing configurations fly best near 25,000 ft. The SC90 and CH90 see some improvements above 25,000 ft, but these are relatively minor. Also, above 25,000 ft, the large-wing configurations are close to their maximum ceiling. In order to leave some additional climb power in cruise, as well as improve convergence in the sizing code, 25,000 ft was chosen as the cruise altitude for the SC90, CH90, and TC90. The SW90 fuel burn and empty weight curves are essentially flat until 16,000 ft and then rise sharply. 15,000 ft was the cruise altitude chosen for the SW90.

For the large-wing designs—the CH90, SC90, and TC90—both wing loading and disk loading were varied to determine the optimum rotor and wing size for minimum fuel burn, empty weight, and installed power. For the SW90, the wing dimensions were left constant, but the disk loading was varied. The effects of disk loading and wing loading are shown in Figs. 14-23.

Figures 14-19 show that the trends for the CH90 and SC90 designs are very similar. A disk loading that is as low as possible is desirable to minimize both fuel burn and engine power. The empty weight is minimized for a disk loading between approximately 10 and 14 lb/ft^2, depending on wing loading, but these curves are quite flat (the scale on Figs. 15 and 18 is magnified to show separation in the results).

Fuel burn for the CH90 and SC90 shows a higher sensitivity to wing loading than it does to disk loading, with a low wing loading providing the best results. The structural weight decrease that results from the reduction in fuel burn and engine power offsets the weight increase of the larger wing, so empty weight is relatively unaffected by changes in wing

loading. A wing loading of 80 lb/ft^2 gives the best combination of fuel burn, empty weight, and engine power for both the CH90 and the SC90.

Wing loading was not varied for the SW90 configuration, so results for fuel burn, empty weight, and engine power are all shown in Fig. 20. Minimum engine power for this design results from a disk loading of 11 lb/ft^2, while a disk loading of 12 lb/ft^2 gives minimum fuel burn and empty weight.

Some practical limitations were set for rotor size for all designs. For the single main rotor configurations, the blade aspect ratio can get very high as the disk loading is lowered. For existing very large helicopters, the upper bound on blade aspect ratio is approximately 20, so this was chosen as the upper limit for the CH90, SC90, and SW90. Applying this limit resulted in a disk loading of 13 lb/ft^2 for all three single main rotor configurations. Fewer rotor blades would result in a lower blade aspect ratio and could allow a lower disk loading, but this study only considered a 7-bladed rotor.

The TC90 results for wing loading and disk loading variations are shown in Figs. 21-23. Again, a low disk loading is desirable to minimize weight, fuel and power. For the tandem configuration, there is a physical limit to how large the rotor radius can be, since the main rotor blades will begin to hit the propellers if disk loading is lowered too far. This limits the TC90 rotor radius to approximately 37 feet, resulting in a disk loading of 10 lb/ft^2. Rotor radius could be increased further if the propellers were placed farther outboard on the wing or possibly behind the wing, but these dimensions were not investigated.

For wing loading variations, 80 lb/ft^2 gives the best combination of fuel burn, empty weight, and installed power. The knee in the curves in Figs. 22 and 23 for wing loading equal to 110 and 120 lb/ft^2 is due to the cruise condition sizing the engines. At these wing loading values, a high cruise speed is required to maintain lift on the small wing, so the speed for best range, V_{br}, is actually at the engines' maximum continuous power rating. The engine power is otherwise relatively unaffected by wing loading, so the value of 80 lb/ft^2 was chosen to balance fuel burn and empty weight.

Off-Design Performance

Once the designs were completed for the four configurations, off-design performance was evaluated. Figures 24-27 show maximum effort curves at design gross weight. Speed for best endurance and best range, as well as maximum speed are presented. The same altitude and speed scales are used in the plots for the sake of comparison. Table 5 contains the maximum speed and altitude for the four designs.

Table 5. Maximum speeds and altitudes at DGW

	CH90	SC90	SW90	TC90
Max Speed, kt	285	278	258	253
Max Altitude, kt	32,000	31,000	18,000	28,000

Payload-range curves were also generated, and are shown in Fig. 28. The calculations for the zero-range point on the payload-range curves assumed zero distance for the climb and cruise segments, but maintained the two reserve segments. Weight for the zero-range point is design gross weight. The range indicated on the abscissa does not include the reserve segments, though these segments were included in the performance calculations.

Maximum payload at zero range is directly related to the fuel burn for the design mission, since the weight carrying capacity at DGW is increased by the amount of fuel removed. The SW90 has the highest maximum payload, and the TC90 the lowest, reflecting the differences in fuel burn between these two designs. For the zero-payload corner of Fig. 28, the large-wing designs have similar maximum ranges, but the SW90 range is higher. This is likely because both the wing and the rotor are overloaded for the design mission and they perform better under a lighter load.

DISCUSSION

Table 2 shows the key characteristics of the four compound helicopter configurations, and Table 3 shows weight details. The tandem compound design performs better than the others in empty weight, fuel burn, and installed engine power. Compared with the baseline, the TC90 configuration reduces fuel burn by 24%, empty weight by 14%, and engine power by 40%.

The TC90 has a hover download fraction that is less than half that of the other two large-wing designs, since the wing is entirely outside the rotor wake, leaving only contributions from the fuselage and horizontal tail. Splitting the lift between two large rotors allows for a lower disk loading, resulting in lower induced power for hover. Finally, there is no power lost to anti-torque in hover, since the moments from the counter-rotating lift rotors cancel each other. Since the engines are sized by only the OEI hover condition, maintaining good hover efficiency is key to reducing the installed power, empty weight, and fuel burn.

The SC90 swiveling tail rotor design also performs better than the baseline CH90. The difference can be attributed to the reduced empty weight achieved by eliminating the rotors on the wing as well as their associated gearboxes and drive shafts. There is an approximately 1,000 lb weight penalty (conversion weights in Table 3) for swiveling the tail rotor, but eliminating the propellers provides a larger weight savings, and the down-spiral of weight results in a more efficient aircraft. Still, the TC90 design reduces fuel burn, empty weight, and engine power by 13%, 11%, and 27%, respectively, when compared with the SC90.

The SW90 has a wing half the size of the SC90 wing, resulting in a low wing weight and a drop in hover download from 7.6% to 4.6% of gross weight. These two factors would result in a more efficient aircraft, except the smaller wing requires a more heavily loaded rotor, resulting in a large

drop in cruise efficiency at high speed. Of the three single-main rotor designs, the SW90 has the lowest empty weight and installed power, but the fuel burn for the design mission is 50% higher than that of the SC90.

A single wing size was studied for the small-wing design, and it is quite possible that there is a more efficient combination of wing size and lift share while maintaining a small wing. It would seem unlikely, however, that any gains would improve this configuration enough to make it a better option than either its large-wing counterpart or the tandem design.

There are additional aspects of the compound helicopter design that were outside the scope of this study, but may be looked at in follow-on work. There were no speed requirements imposed, meaning that the cruise speed for the design mission was optimized for efficiency, and the OEI hover requirement sized the engines. For a compound helicopter to be a viable option as a passenger transport, a minimum speed requirement may be necessary. Rotor optimization was limited to blade twist and disk loading, but variations in other rotor characteristics, such as planform, tip speed, and the number of rotor blades could possibly produce a more efficient aircraft. Other mission parameters, such as range and number of passengers, should also be evaluated, and the costs calculated on a per seat-mile basis. Also, while the tandem configuration provides the best performance for the 90-passenger aircraft size studied here, it is not necessarily the best choice for a much smaller aircraft.

SUMMARY AND CONCLUSIONS

Four compound helicopter designs were generated using a combination of rotorcraft sizing and comprehensive analysis software. All four aircraft use both lift and propulsive thrust compounding as well as a slowed main rotor in cruise. The designs include a tandem configuration and three single-main-rotor aircraft. The single-main-rotor designs use either a swiveling tail rotor or wing-mounted propellers for auxiliary propulsion, and both large and small wing sizes were investigated. All four configurations are capable of transporting 90 passengers over a 500 nm design mission at speeds of at least 225 kt.

The competitiveness of the different configurations was evaluated based on fuel burn, empty weight and installed engine power. Rotor optimization included variations in twist and in the balance of lift between the rotor and the wing. Wing loading and disk loading were varied along with cruise altitude to obtain optimum designs for each configuration.

The results lead to the conclusion that for the given civil transport mission, a design using two lifting rotors in a tandem configuration with a large wing and two wing-mounted propellers provides the best performance of the configurations studied. For the design mission and conditions imposed for this study, the one-engine-inoperative hover condition determines the engine size. For this reason, it is important to have very good hover efficiency. The geometry of the tandem configuration allows for a low disk loading and low hover download, providing good takeoff performance, while maintaining acceptable cruise characteristics.

ACKNOWLEDGMENTS

The authors would like to thank Alexander Amy of NASA Ames Research Center for preparing the aircraft drawings.

REFERENCES

1. Couluris, G., Hange, C., Wardwell, D., Signor, D., and Phillips, J., "A Potential Impact Analysis of ESTOL Aircraft on Newark Airport Operations," American Institute of Aeronautics and Astronautics Modeling and Simulation Technologies Conference and Exhibit, Hilton Head, SC, August 20-23, 2007.

2. Chung, W., Linse, D., Paris, A., Salvano, D., Trept, T., Wood, T., Gao, H., Miller, D., Wright, K., Young, R., Cheng, V., "Modeling High-Speed Civil Tiltrotor Transports in the Next Generation Airspace," NASA/CR-2011-215960, October 2011.

3. Johnson, W., Yamauchi, G., and Watts, M., "NASA Heavy Lift Rotorcraft Systems Investigation," NASA TP-2005-213467, December 2005.

4. Russell, C. and Johnson, W., "Conceptual Design and Performance Analysis for a Large Civil Compound Helicopter," AHS Future Vertical Lift Aircraft Design Conference, San Francisco, CA, January 18-20, 2012.

5. Taylor, J., *Jane's All the World's Aircraft, 1969-70*. London: Jane's Yearbooks, 1969.

6. Walsh, D., Weiner, S., Arifian, K., Lawrence, T., Wilson, M., Millott, W., and Blackwell, R., "High Airspeed Testing of the Sikorsky X2 Technology™ Demonstrator," American Helicopter Society 67th Annual Forum, Virginia Beach, VA, May 2011.

7. "Aviation Week Flies Eurocopter's X3," *Aviation Week & Space Technology*, July 9, 2012.

8. Yeo, H. and Johnson, W., "Optimum Design of a Compound Helicopter," *Journal of Aircraft*, Vol. 46, No. 4, July-August 2009.

9. Moodie, A. and Yeo, H., "Design of a Cruise Efficient Compound Helicopter," American Helicopter Society 67th Annual Forum, Virginia Beach, VA, May 3-5, 2011.

10. Silva, C., Yeo, H., and Johnson, W., "Design of a Slowed-Rotor Compound Helicopter for Future Joint Service Missions," American Helicopter Society Aeromechanics Specialists' Conference, San Francisco, CA, January 20-22, 2010.

11. Johnson, W., Moodie, A., and Yeo, H., "Design and Performance of Lift-Offset Rotorcraft for Short-Haul Missions," American Helicopter Society Future Vertical Lift Aircraft Design Conference, San Francisco, CA, January 2012.

12. Acree, C.W., Jr., Yeo, H. and Sinsay, J., "Performance Optimization of the NASA Large Civil Tiltrotor," International Powered Lift Conference, London, UK, July 22-24, 2008.

13. Yeo, H., Sinsay, J. and Acree, C. W., Jr., "Selection of Rotor Solidity for Heavy Lift Tiltrotor Design," *Journal of the American Helicopter Socieity*, Vol. 55, No. 1, January 2010.

14. Johnson, W. "NDARC. NASA Design and Analysis of Rotorcraft." NASA TP 2009-215402, December 2009.

15. Johnson, W. "NDARC — NASA Design and Analysis of Rotorcraft. Theoretical Basis and Architecture." American Helicopter Society Specialists' Conference on Aeromechanics, San Francisco, CA, January 2010.

16. Johnson, W. "NDARC — NASA Design and Analysis of Rotorcraft. Validation and Demonstration." American Helicopter Society Specialists' Conference on Aeromechanics, San Francisco, CA, January 2010.

17. Harris, F. B., "Rotor Performance at High Advance Ratio; Theory versus Test," NASA CR 2008-215370, October 2008.

18. Johnson, W., "Technology Drivers in the Development of CAMRAD II," American Helicopter Society Aeromechanics Specialist Meeting, San Francisco, California, January 1994.

19. Johnson, W. "Rotorcraft Aeromechanics Applications of a Comprehensive Analysis." HeliJapan 1998: AHS International Meeting on Rotorcraft Technology and Disaster Relief, Gifu, Japan, April 1998.

20. Johnson, W. "Rotorcraft Aerodynamic Models for a Comprehensive Analysis." American Helicopter Society 54th Annual Forum, Washington, D.C., May 1998.

21. Johnson, W. "Calculation of Tilt Rotor Aeroacoustic Model (TRAM DNW) Performance, Airloads, and Structural Loads." American Helicopter Society Aeromechanics Specialists' Meeting, Atlanta, GA, November 2000.

22. Yeo, H. "Calculation of Rotor Performance and Loads Under Stalled Conditions." American Helicopter Society 59th Annual Forum, Phoenix, AZ, May 2003.

23. Yeo, H., Bousman, W. G., and Johnson, W., "Performance Analysis of a Utility Helicopter with Standard and Advanced Rotor," *Journal of the American Helicopter Society*, Vol. 49, No. 3, July 2004.

24. Yeo, H., and Johnson, W., "Assessment of Comprehensive Analysis Calculation of Airloads on Helicopter Rotors," *Journal of Aircraft*, Vol. 42, No. 5, Sept.–Oct. 2005.

25. Yeo, H., and Johnson, W., "Prediction of Rotor Structural Loads with Comprehensive Analysis," *Journal of the American Helicopter Society*, Vol. 53, No. 2, April 2008.

26. Harris, F.D. "Rotor Performance at High Advance Ratio; Theory versus Test." NASA CR 2008-215370, October 2008.

Table 2. Design summary for four compound helicopter configurations

	CH90	SC90	SW90	TC90
Payload (90 pax), lb	19,800	19,800	19,800	19,800
Max takeoff weight, lb	115,680	103,167	105,607	93,794
Design gross weight, lb	100,592	89,711	91,832	81,663
Empty weight, lb	67,382	57,952	54,931	51,343
Mission fuel, lb	11,964	10,494	15,654	9,137
Engine max rated power, hp	4×7,225	4×5,966	4×5,846	4×4,366
Hover download, DL/W	7.3%	7.6%	4.6%	3.3%
Design mission cruise speed, kt	230	231	225	231
Cruise L/D_e, WV/P	7.8	7.8	4.8	8.0
Main rotor disk loading, lb/ft^2	13.0	13.0	13.0	10.0
Main rotor solidity	0.112	0.112	0.112	0.0860
Main rotor design C_W/σ	0.151	0.151	0.151	0.151
Main rotor radius, ft	49.6	46.9	47.4	36.1
Main rotor V_{tip}, hover, ft/s	650	650	650	650
Main rotor V_{tip}, cruise, ft/s	450	450	550	475
Main rotor number of blades	7	7	7	4
Main rotor 1 incidence, deg	2.0	2.0	3.0	1.9
Main rotor 2 incidence, deg	—	—	—	2.9
Tail rotor radius, ft	8.6	10.3	10.3	—
Propeller radius, ft	7.0	—	—	7.0
Wing lift share in cruise	85%	85%	50%	85%
Wing span, ft	125.4	118.4	50.0	113.0
Wing area, ft^2	1,257	1,121	554	1,021
Wing loading, lb/ft^2	80.0	80.0	166.0	80.0
Wing incidence, deg	1.6	1.6	4.1	2.2

Table 3. Weights for four compound helicopter configurations

	CH90		SC90		SW90		TC90	
	Weight (lb)	%DGW	Weight (lb)	%DGW	Weight (lb)	%DGW	Weight (lb)	%DGW
WEIGHT EMPTY	67382	67.0	57952	64.6	54931	59.8	51343	62.9
STRUCTURE	29685	29.5	26331	29.4	23254	25.3	22687	27.8
wing group	8641	8.6	7649	8.5	4022	4.4	6853	8.4
rotor group	5885	5.9	5064	5.6	5222	5.7	4575	5.6
horizontal tail	252	0.3	205	0.2	214	0.2	295	0.4
vertical tail	175	0.2	149	0.2	154	0.2	—	—
tail rotor	1621	1.6	1377	1.5	1583	1.7	—	—
fuselage group	8734	8.7	8065	9.0	8197	8.9	7677	9.4
alighting gear	2418	2.4	2156	2.4	2207	2.4	1963	2.4
engine section	1794	1.8	1531	1.7	1525	1.7	1231	1.5
air induction	166	0.2	133	0.1	130	0.1	93	0.1
PROPULSION GROUP	21009	20.9	14716	16.4	14927	16.3	13627	16.7
engine system	3975	4.0	3293	3.7	3228	3.5	2428	3.0
propellers	1752	1.7	—	—	—	—	1752	2.1
fuel system	1660	1.7	1482	1.7	1846	2.0	1281	1.6
drive system	13622	13.5	9941	11.1	9853	10.7	8166	10.0
SYSTEMS AND EQUIPMENT	12647	12.6	13428	15.0	13454	14.7	11948	14.6
flight controls	795	0.8	1659	1.8	1691	1.8	854	1.0
conversion	—	—	917	1.0	939	1.0	—	—
auxiliary power	600	0.6	600	0.7	600	0.7	600	0.7
instruments group	150	0.1	150	0.2	150	0.2	150	0.2
hydraulic group	108	0.1	300	0.3	306	0.3	114	0.1
conversion	—	—	200	0.2	204	0.2	—	—
electrical group	3582	3.6	3402	3.8	3441	3.7	3042	3.7
avionics	800	0.8	800	0.9	800	0.9	800	1.0
furnishings & equipment	4000	4.0	4000	4.5	4000	4.4	4000	4.9
environmental controls	1685	1.7	1685	1.9	1685	1.8	1685	2.1
anti-icing group	926	0.9	832	0.9	780	0.8	703	0.9
CONTINGENCY	4043	4.0	3477	3.9	3296	3.6	3081	3.8
FIXED USEFUL LOAD	1440	1.4	1440	1.6	1440	1.6	1440	1.8
crew	1100	1.1	1100	1.2	1100	1.2	1100	1.3
other fixed useful load	340	0.3	340	0.4	340	0.4	340	0.4
OPERATING WEIGHT	68823	68.4	59392	66.2	56371	61.4	52783	64.6

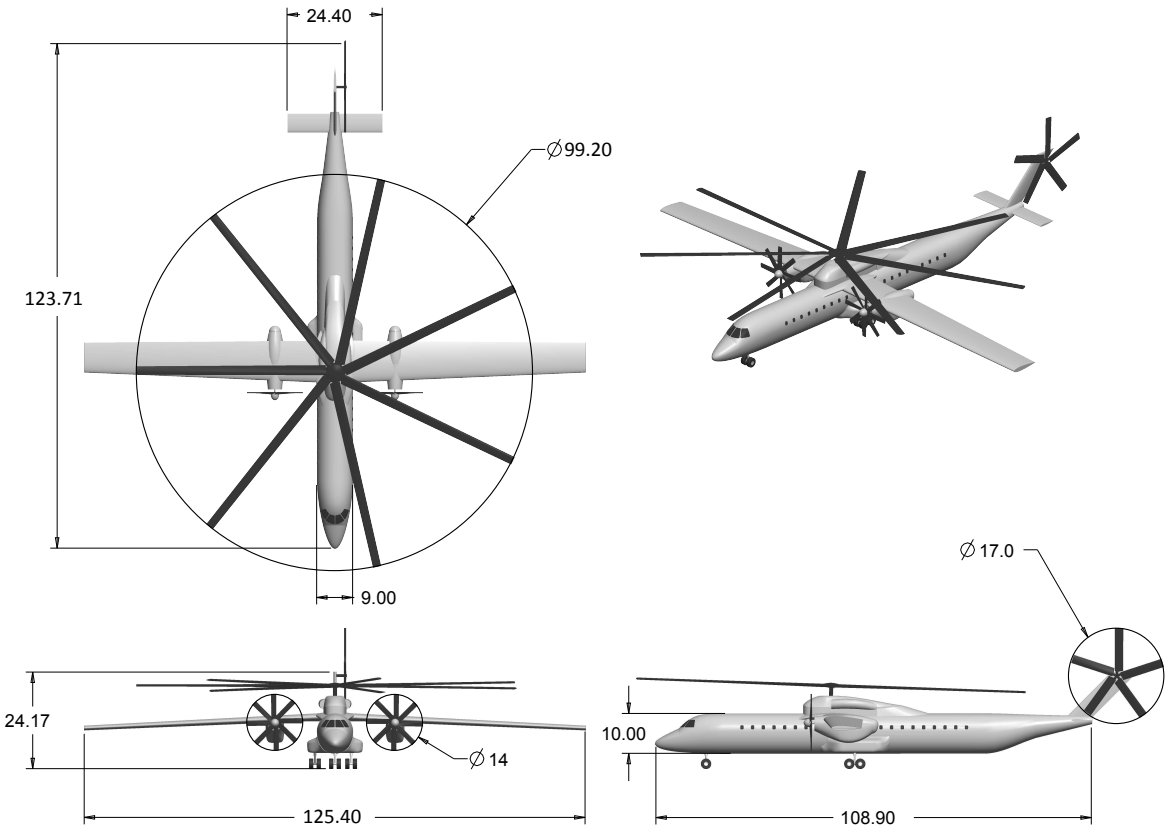

Figure 1. Illustration of the baseline compound helicopter, CH90

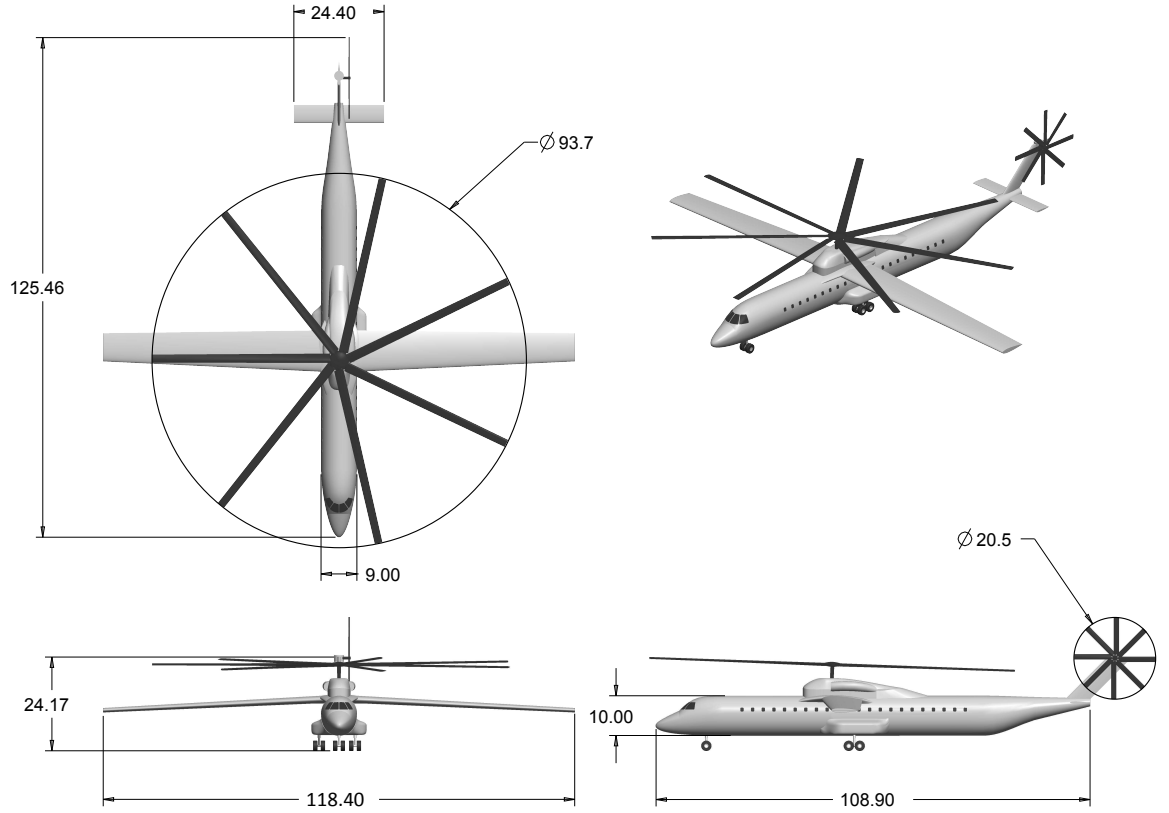

Figure 2. Illustration of the swiveling tail rotor compound helicopter, SC90

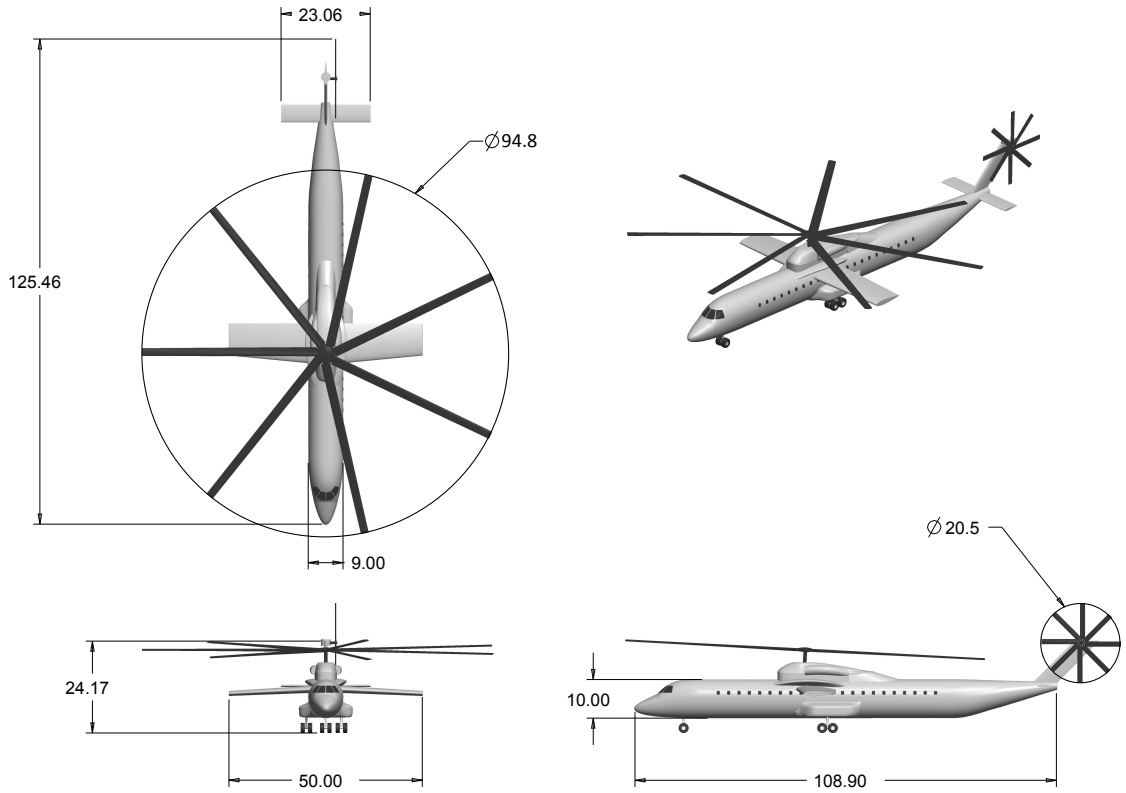

Figure 3. Illustration of the small-wing compound helicopter, SW90

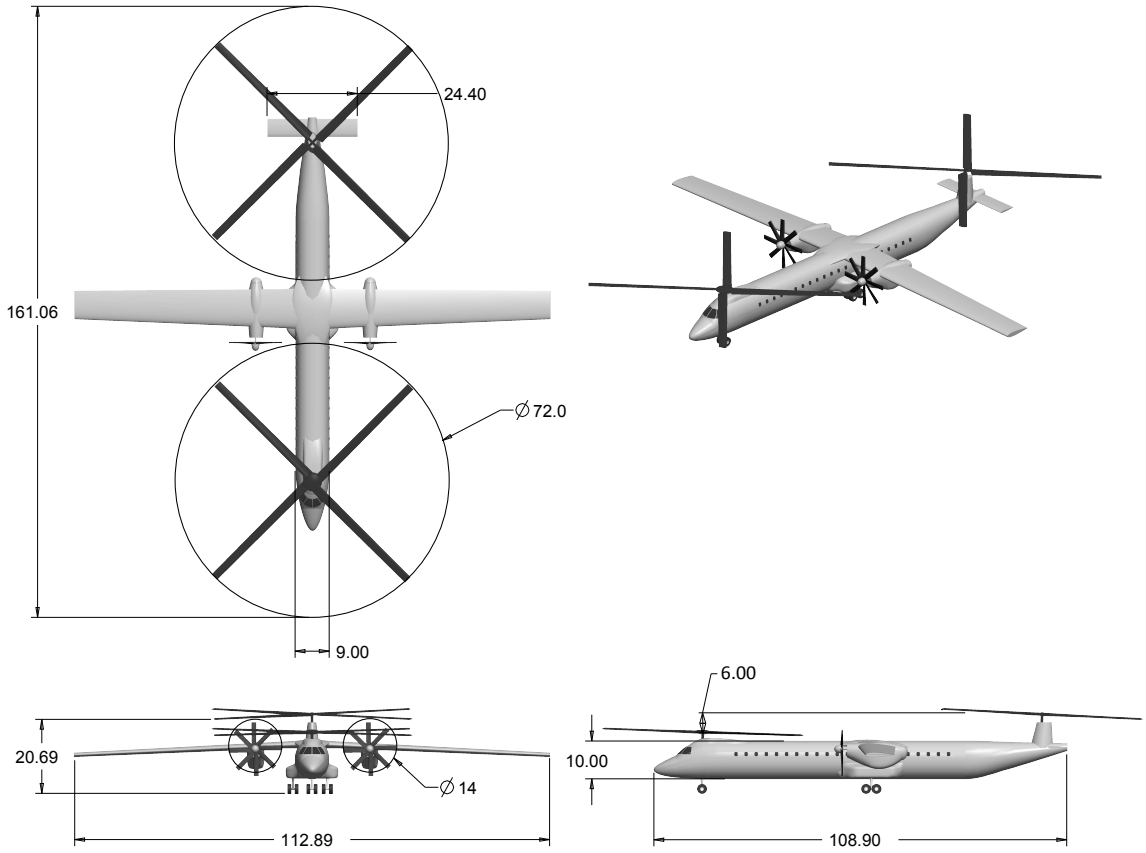

Figure 4. Illustration of the tandem compound helicopter, TC90

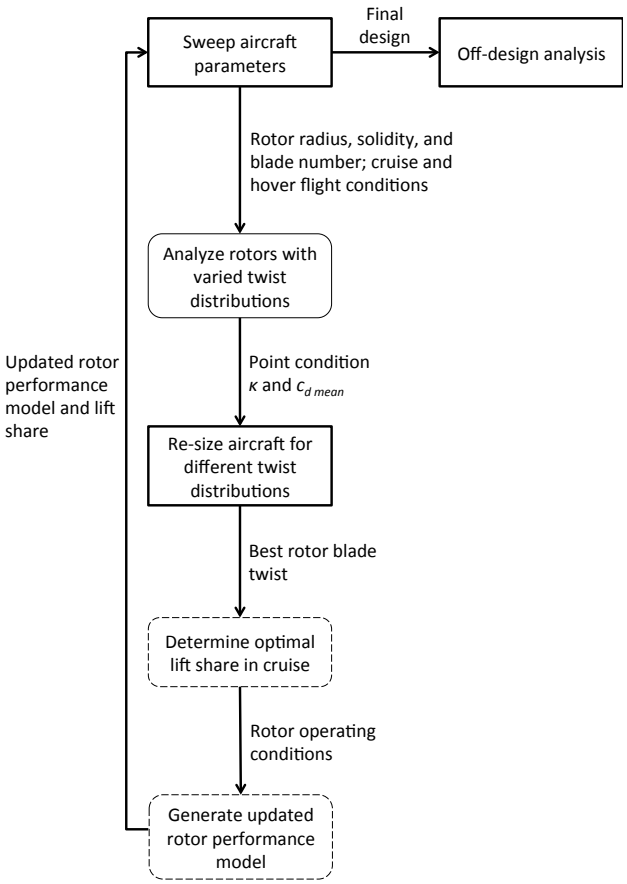

Figure 5. Iterative design process. NDARC tasks in square boxes, and CAMRAD II tasks in rounded boxes. Tasks using both CAMRAD II and spreadsheet analysis contained in dashed rounded boxes

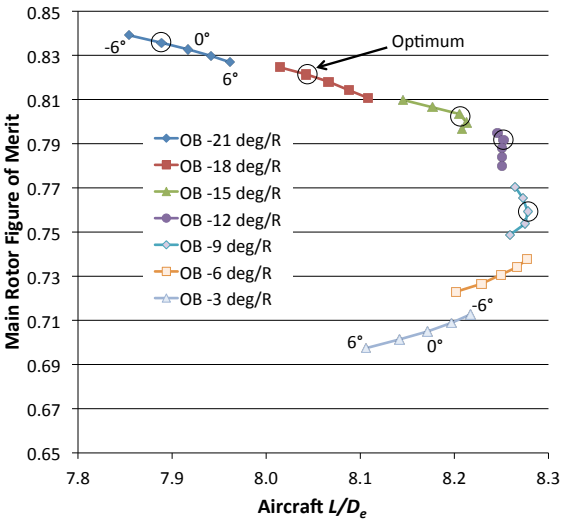

Figure 6. SC90 and CH90 main rotor figure of merit and aircraft L/D_e for varied inboard and outboard twist rates

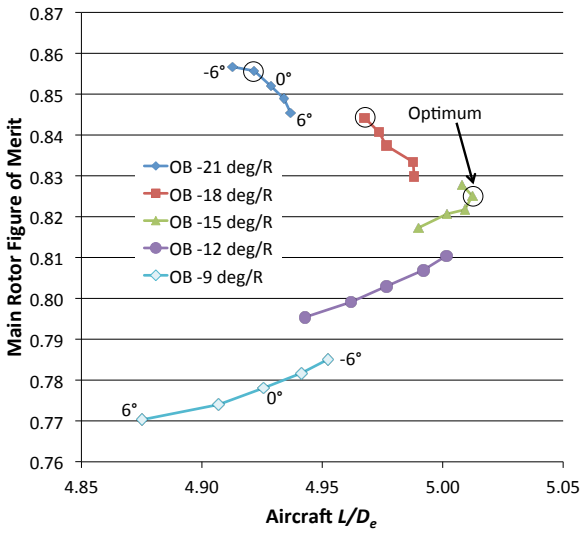

Figure 7. SW90 main rotor figure of merit and aircraft L/D_e for varied inboard and outboard twist rates

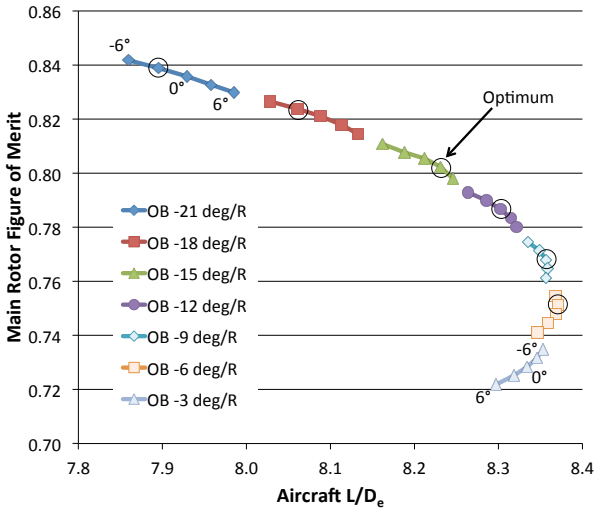

Figure 8. TC90 main rotor figure of merit and aircraft L/D_e for varied inboard and outboard twist rates

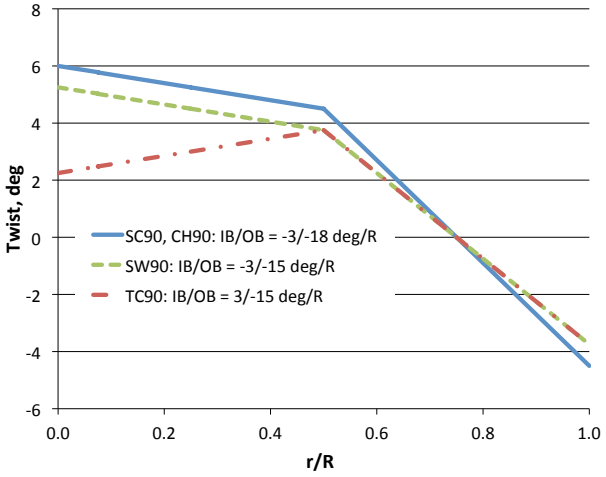

Figure 9. Main rotor bi-linear twist distribution as a function of radial location; curves identified by inboard/outboard twist rate in °/R

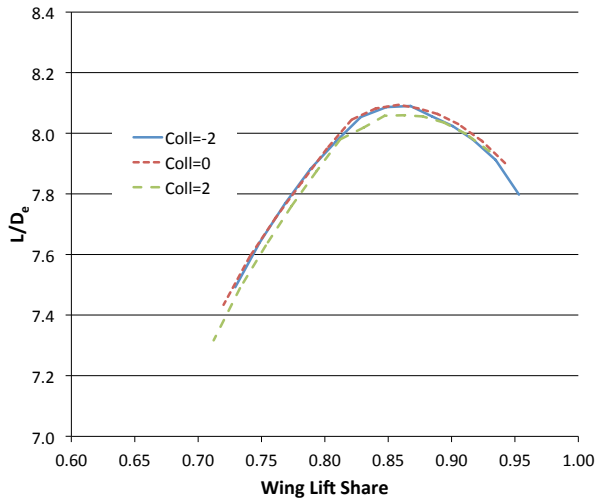

Figure 10. Effective lift-to-drag ratio vs. wing lift share for the SC90 and CH90 configurations

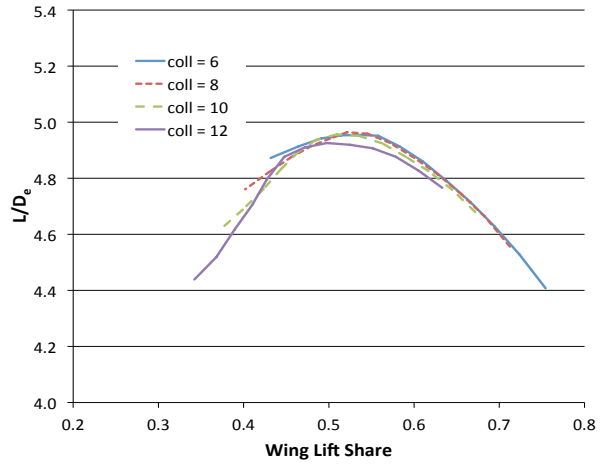

Figure 11. Effective lift-to-drag ratio vs. wing lift share for the SW90 configuration

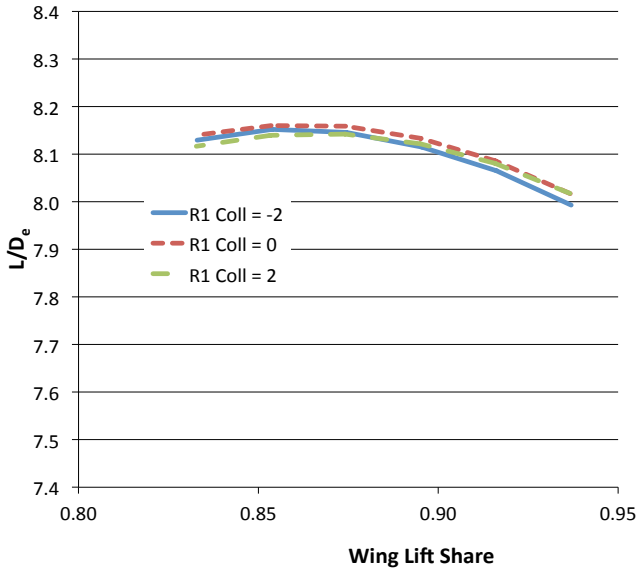

Figure 12. Effective lift-to-drag ratio vs. wing lift share for the TC 90 configuration

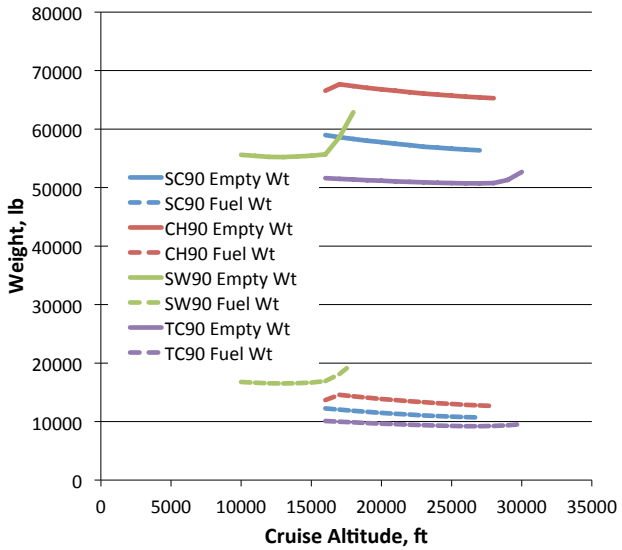

Figure 13. Effects of cruise altitude on empty weight and fuel burn for the four compound configurations

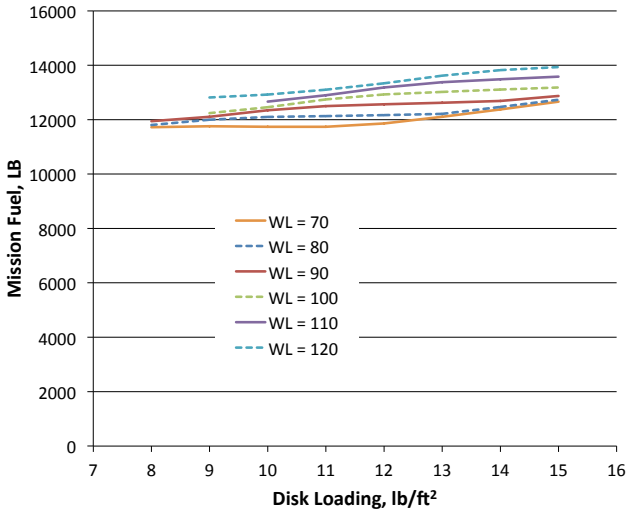

Figure 14. CH90 mission fuel as a function of wing loading and disk loading

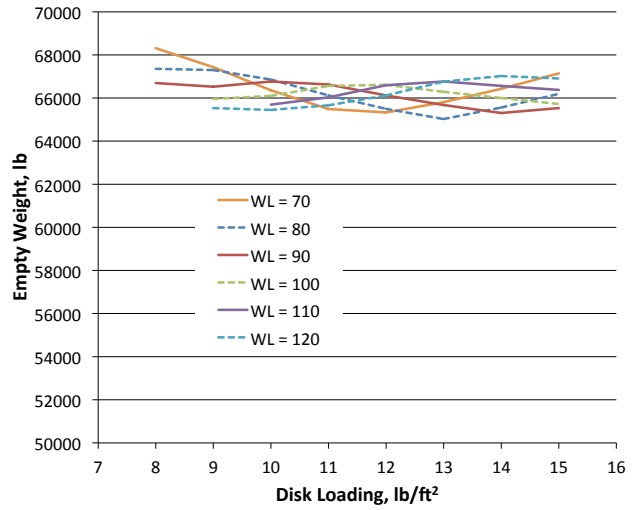

Figure 15. CH90 empty weight as a function of wing loading and disk loading

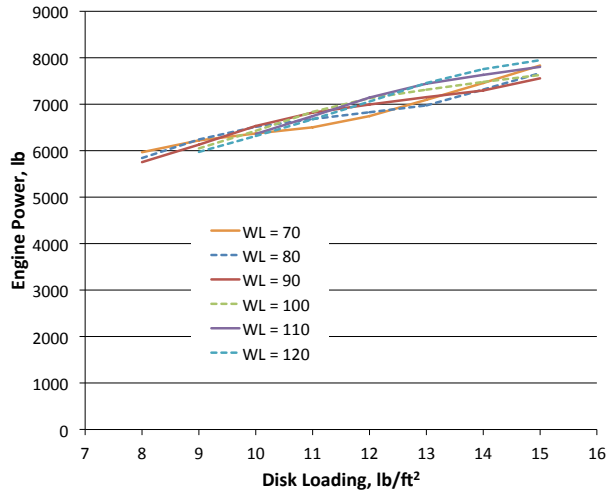

Figure 16. CH90 maximum rated power per engine as a function of wing loading and disk loading

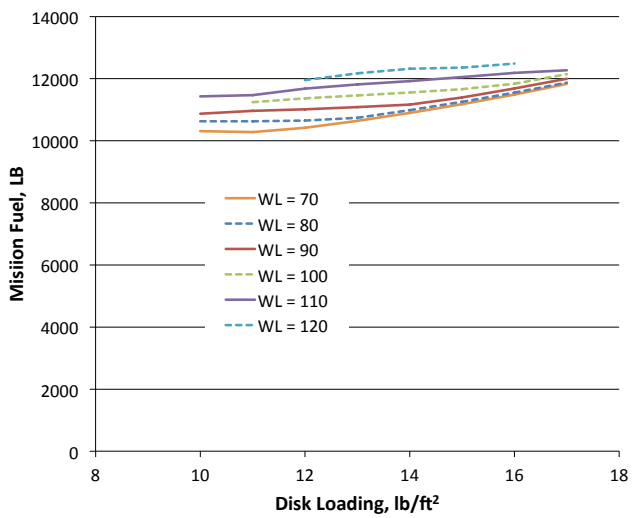

Figure 17. SC90 mission fuel as a function of wing loading and disk loading

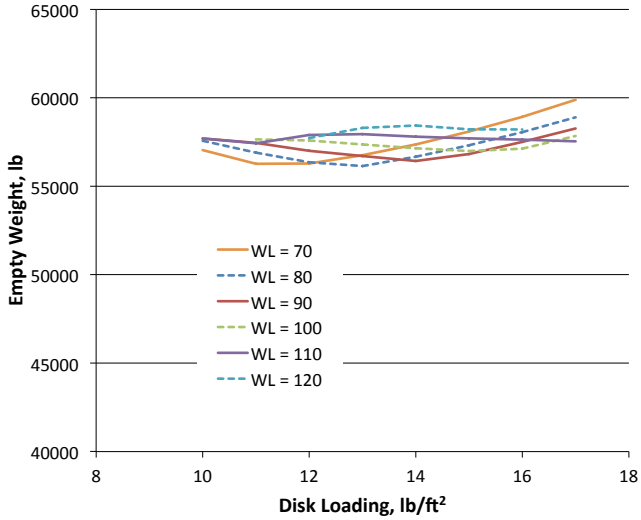

Figure 18. SC90 empty weight as a function of wing loading and disk loading

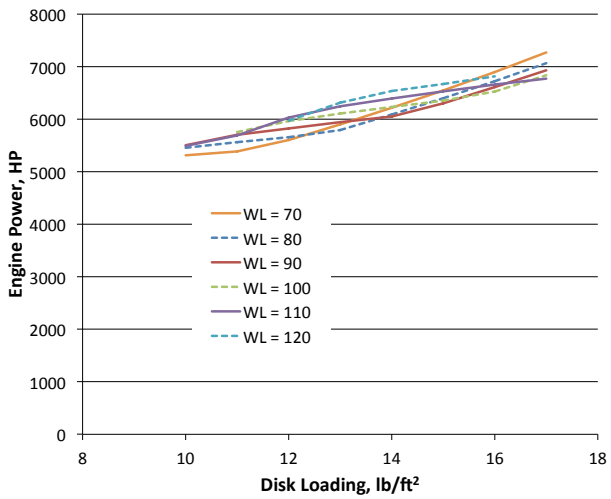

Figure 19. SC90 maximum rated power per engine as a function of wing loading and disk loading

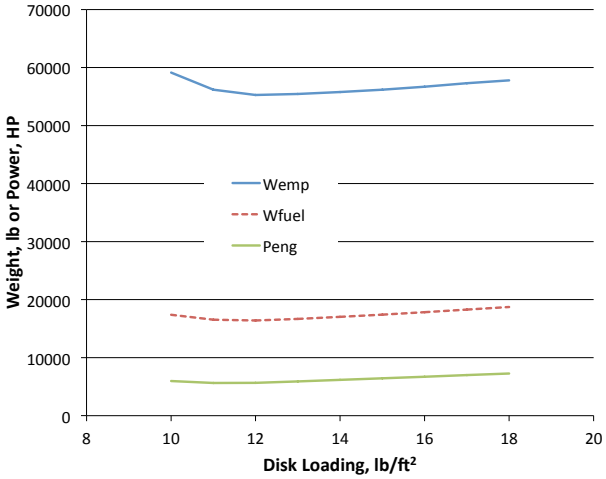

Figure 20. SW90 mission fuel, empty weight, and maximum rated power per engine as a function of disk loading

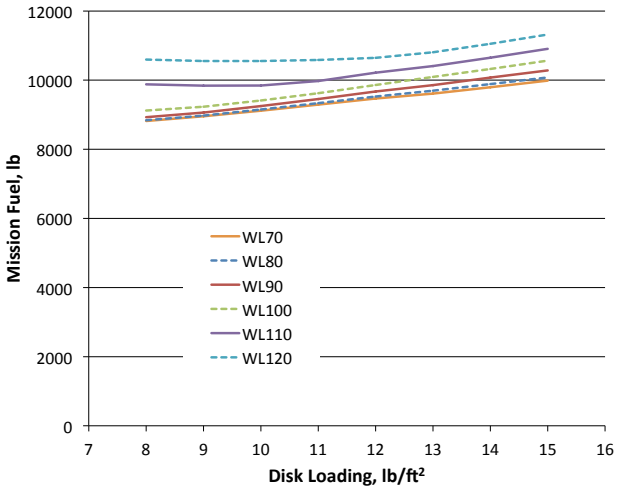

Figure 21. TC90 mission fuel as a function of wing loading and disk loading

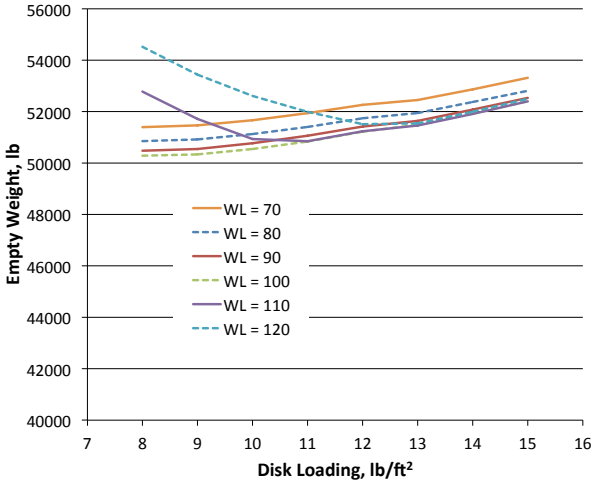

Figure 22. TC90 empty weight as a function of wing loading and disk loading

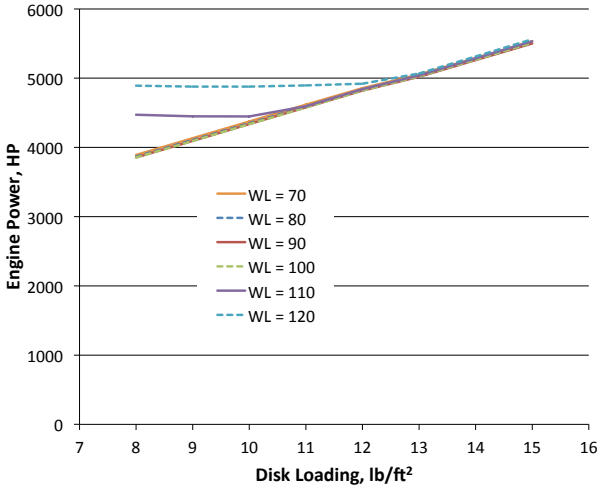

Figure 23. TC90 maximum rated power per engine as a function of wing loading and disk loading

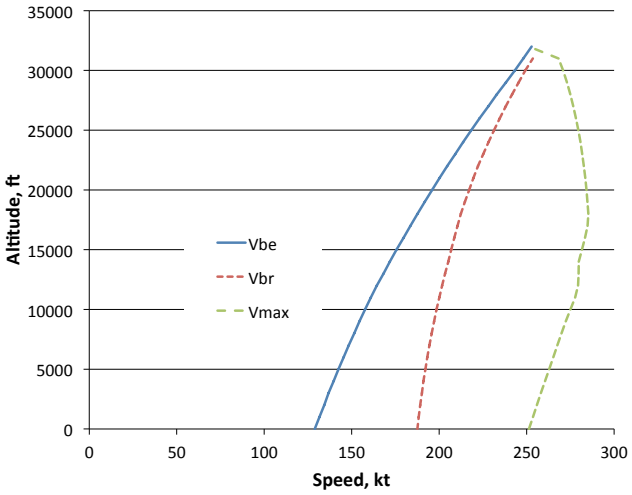

Figure 24. CH90 speed for best endurance (V_{be}), best range (V_{br}) and maximum speed (V_{max})

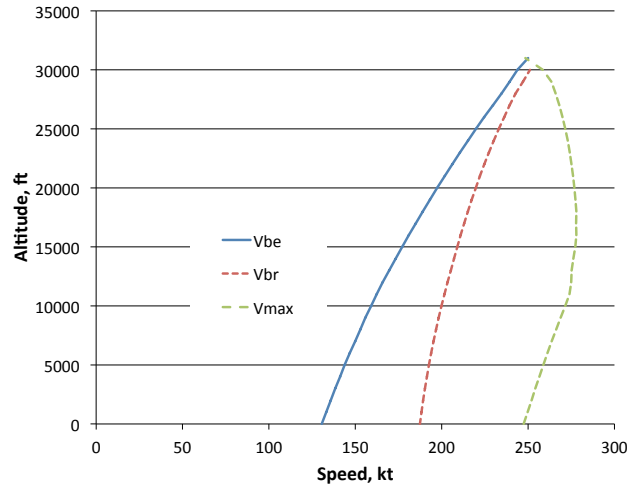

Figure 25. SC90 speed for best endurance (V_{be}), best range (V_{br}) and maximum speed (V_{max})

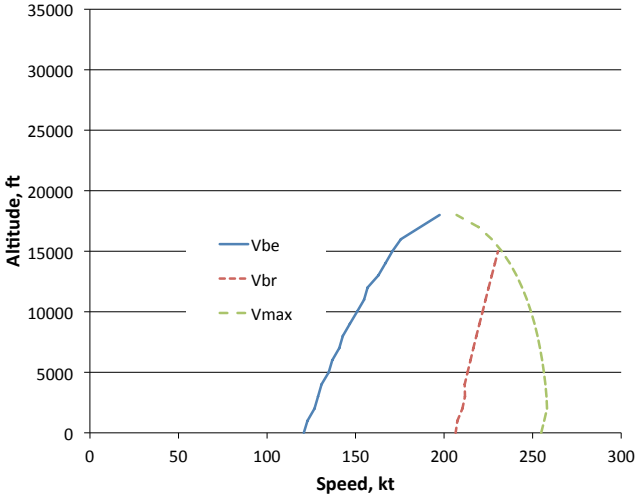

Figure 26. SW90 speed for best endurance (V_{be}), best range (V_{br}) and maximum speed (V_{max})

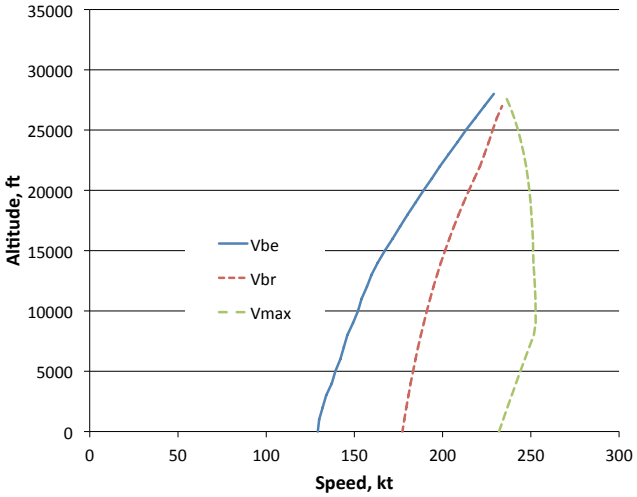

Figure 27. TC90 speed for best endurance (V_{be}), best range (V_{br}) and maximum speed (V_{max})

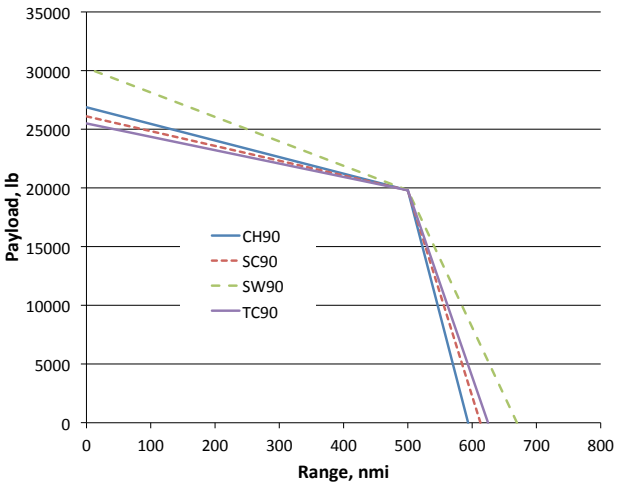

Figure 28. Payload-range curves for the four designs with 5k ISA +20°C takeoff; zero range takeoff at DGW